Asian Journal of Chemistry; Vol. 32, No. 10 (2020), 2520-2528

ASIAN JOURNAL OF CHEMISTRY

https://doi.org/10.14233/ajchem.2020.22820

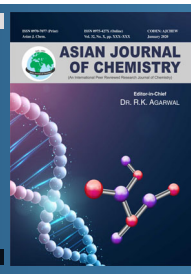

Synthesis of $SrTiO_3$ Nanotubes from Green TiO_2 Nanoparticles for Enhanced Photocatalytic Activity

K.S. KIRAN[1], ASHWATH NARAYANA[2] and S.V. LOKESH[1,*]

[1]Department of Nanotechnology, Centre for Post Graduate Studies-Bangalore Region, Visvesvaraya Technological University, Muddenahalli, Chikkaballapur-562101, India
[2]Department of Bio-Medical Engineering, Rajiv Gandhi Institute of Technology, Cholanagar, R.T. Nagar, Hebbal, Bengaluru-560032, India

*Corresponding author: E-mail: lokeshsampangi@gmail.com

Received: 7 May 2020; *Accepted*: 8 June 2020; *Published online*: 25 September 2020; AJC-20063

The strontium titanate ($SrTiO_3$) nanotubes with perovskite structure was incorporated utilizing hydrothermal synthesis approach were examined with their photo catalytic activity. The TiO_2 nanoparticles employed in synthesis of $SrTiO_3$ nanotubes were synthesized prior using *Azadirachta indica* leaf extract commonly termed as green synthesis. $SrTiO_3$ nanotubes with bandgap of 3.25 eV (purest form of semiconductor) showed the much better photocurrent intensity was attributed to the more homogenous and nanotube formation with perovskite structure and greater surface area with maximum light retention property. The $SrTiO_3$ nanotubes obtained at much lower temperature of 150 ºC were characterized by XRD, TEM, FESEM, EDAX and FTIR analysis. Herein, we report the strontium titanate ($SrTiO_3$) nanotubes as active photocatalyst and their kinetics study were performed for first order rate constant which confirmed the photodegradation of methylene blue dye in 90 min under UV light and 150 min under natural sunlight (visible) irradiation at ambient temperature.

Keywords: *Azadirachta indica*, TiO_2, Strontium titanate, Photocatalytic activity, Methylene blue, Perovskite structure.

INTRODUCTION

The interest for vitality and ascend in barometrical temperature are trying to advance new materials for most extreme usage of sunlight based insolation. Generally, the reactant execution of fine particles is impacted by the crystal phase, size, surface area and crystallinity. Strontium titanate ($SrTiO_3$) is a very much recognized with a bandgap of 3.25 eV having cubic-perovskite type structure, possesses unrivaled chemical stability and is known substrate for the epitaxial development of different perovskite oxides with assorted properties [1,2]. $SrTiO_3$ in purest form of semiconductor has 3.25 eV (indirect bandgap) and 3.75 eV (direct bandgap) and furthermore as a quantum (ferroelectric) material. The dielectric constant of material increases (~10^4) as temperature decreases and then remains constant below 4 K. Inorganic perovskites has gained interest of researchers as a promising semiconductor, photocatalyst as a result of its structural simplicity, excellent stability, brilliant steadiness and the simple incorporation of different metallic elements in the lattices [3-5]. The perovskites materials with excellent outperforming and mechanical interests have gained attention for their utilization as a photocatalyst in catalysis [6], in photovoltaic cells, electron transport material [7]. The $SrTiO_3$ nanotubes can be synthesized by numerous approaches such as hydrothermal, electrospinning technique, sol-gel, *etc*. [8-10].

Regardless of the broad research endeavors, control of their size and shape has not been sufficiently accomplished yet. Rheinheimer and Hoffmann [11] portrayed a convention to blend stoichiometric strontium titanate powder utilizing blended oxide/carbonate course dependent on crude materials (TiO_2 and $SrCO_3$). Novel permeable Cr-doped $SrTiO_3$ nanotubes were synthesized by utilizing a basic and monetary electrospinning procedure for visible light driven photocatalytic activity which evaluated by degradation of azo dye acid orange 7 and removal of NO under visible light irradiation for nearly ~240 min [12]. Strontium titanate has appropriate band structures for water splitting whereas TiO_2 is widely used for water splitting by UV light and this was first exhibited by Fujishima and Honda [13] utilizing a TiO_2 photo-electrode by applying an external bias. Rather than TiO_2, $SrTiO_3$ photoelectrodes can split water without

providing an electric bias as a result of the more appropriate band structure of titanate [14]. Its high thermodynamic strength is further leeway of strontium titanate; it doesn't decay under lessening conditions even at high temperature, in an unexpected way from numerous other oxide perovskites, and shows great chemical and redox stability.

In spite of various synthesis methods the hydrothermal synthesis approach has two fundamental points of interest: (i) it empowers the readiness of exceptionally unadulterated and incredibly fine powders with high explicit surface area; (ii) the particle size and morphology can be effortlessly controlled and structured by changing the response time, temperature, nature of precursor and concentration of precursor [15]. As photocatalyst strontium titanate has gained key attention to researchers in the degradation of organic and inorganic compounds and reduction of CO_2 [16-18]. For photosensitized solar based devices $SrTiO_3$ is used as a photoelectrode material, which has been investigated many researchers all over the world, owing to the fact that it is less proficient than TiO_2 anatase [19]. Hydrothermal is the general process for synthesis of $SrTiO_3$ by reacting TiO_2 powder (rutile or amorphous or anatase titania) with a soluble Sr salt such as $SrCl_2$, $Sr(OH)_2$, $Sr(NO_3)_2$ maintaining under highly alkaline nature [15,20-22].

Herein, strontium titanate ($SrTiO_3$) nanotubes were synthesized using hydrothermal synthesis approach which is simple, economic and easy synthesis process. Using the lower initiation temperature of 150 ºC strontium titanate nanotubes were synthesized by incorporating the TiO_2 nanoparticles into strontium nitrate $Sr(NO_3)_2$ in autoclave for 22 h. The photocatalytic activity of $SrTiO_3$ nanotubes and their kinetics study were performed for first order rate constant, which confirmed the methylene blue photodegradation in 90 min under UV and in 150 min under natural sunlight (visible) irradiation at ambient temperature.

EXPERIMENTAL

AR grade titanium(IV) isopropoxide with 97% purity (Sigma-Aldrich), $Sr(NO_3)_2$ with 99.9% purity (Sigma-Aldrich), TiO_2 99% purity (Loba Chemie), NaOH pellets and HCl 32% AR grade and ethyl alcohol 99.9% (S.D. Fine Chemicals) were procured for the synthesis of TiO_2 nanoparticles and $SrTiO_3$ nanotubes.

Preparation of aqueous *Azadirachta indica* leaf extract: *A. indica* (Neem) leaves were collected and cleaned with fresh water followed by deionized water as initial cleaning process and dried with hot air gun at room temperature. The leaves were shredded into pieces nearly 50 g were put in 200 mL beaker containing 100 mL of deionized water. The resultant mixture was heated at 110 ºC on a hot plate (magnetic stirrer) under continuous stirring for 4 h leading to the formation of greenish solution. The so obtained extract was then filtered using filter paper grade 1 (Whatman) in a different beaker allowing it cool at room temperature, resulting dark greenish solution of *Azadirachta indica* leaf extract, which was further used in synthesis of TiO_2 nanoparticles.

Synthesis of TiO_2 nanoparticles: Initially, titanium (IV) isopropoxide of 2 mL was added to 20 mL of *Azadirachta indica* leaf extract and continuously stirred using magnetic stirrer with 400 rpm for 30 min at room temperature. The resultant solution was further transferred to silica crucible and heated at 150 ºC using electric bunsen burner leading to the formation of TiO_2 nanoparticles as titanium(IV) isopropoxide reacts with *Azadirachta indica* leaf extract leaving other components to evaporate. The resultant powder was dried at 120 ºC for 2 h and then fine grinded for 5 min in an agate mortar and was made available to utilize for the synthesis of $SrTiO_3$ nanotubes.

Synthesis of $SrTiO_3$ nanotubes: The as-synthesized TiO_2 nanoparticles (0.8 g) was added to the solution prepared prior by adding 10 g of NaOH in 25 mL of deionized water under continuous stirring with 400 rpm for 15 min at room temperature and stirring was continued after adding TiO_2 nanoparticles for next 15 min. The resultant mixture was further added with 1.5 g of $Sr(NO_3)_2$ allowing the stirrer to stir the mixture with 800 rpm for 30 min maintaining room temperature of 26 ºC with relative humidity of 40%. The ensuing solution was further transferred to Teflon lined stainless steel autoclave of 60 mL capacity and heated at 150 ºC for 22 h and then cooled to room temperature for the next process of neutralizing the pH value by washing the mixture with deionized water and 0.1M of HCl followed by ethyl alcohol for several times by centrifuging until it reaches neutral pH and was then dried at 80 ºC overnight in vacuum oven. After fine grinding the obtained nanotubes using agate mortar for 1 h without any further delay the sample was transferred to glass bottle (amber sample) at room temperature. The complete synthesis process of TiO_2 nanoparticles and $SrTiO_3$ nanotubes schematic representation is shown in Fig. 1.

RESULTS AND DISCUSSION

XRD studies: XRD pattern recorded of the as-synthesized TiO_2 nanoparticles at room temperature using Rigaku Ultima IV X-ray diffractometer in the 2θ range of 10º-70º is depicted in Fig. 2a indicating several clear diffraction peaks confirming the TiO_2 nanoparticles. The major peaks along (101), (103), (004), (112), (200), (105), (211), (204) and (116) crystallographic planes was the Bragg's reflection corresponding to 2θ values 25.3º, 37.8º, 38.0º, 38.6º, 48.0º, 53.9º, 55.0º, 62.7º and 68.8º which was in good agreement with anatase phase of TiO_2 nanoparticles (anatase XRD JCPDS card no. 21-1272). The crystallite size was extracted using the peaks and calculated using Scherrer's formula ($D = k\lambda/(\beta\cos\theta)$) where, λ is the wavelength (CuKα = 0.1548 nm), K is a constant (0.89), β is full width at half maximum (FWHM) and θ is the diffracting angle. The as-synthesized TiO_2 nanoparticles average crystalline size was found to be ~ 70 nm. Similarly, the XRD patterns of TiO_2 NPs employed $SrTiO_3$ nanotube is shown in Fig. 2b. The as-synthesized $SrTiO_3$ at room temperature crystallizes in the ABO_3 cubic perovskite structure (space group P*m*3*m*) with a lattice parameter of 3.90 Å and $\rho = 5.12$ g/cm^3 as density [23]. The crystalline nature of $SrTiO_3$ was confirmed by the existence of strong sharp peak and the notable peaks along (110), (111), (200), (211) and (220) corresponding to the peaks occurring at 2θ values 32.2º, 39.8º, 45.7º, 57.6º and 66.9º (JCPDS card no.: 35-0734) confirmed the ABO_3 cubic perovskite structure, which is good accord with published values [24]. Similarly, the as-synthesized $SrTiO_3$ nanotubes average crystalline size was determined using Scherrer's formula and found to be approximately 14 nm.

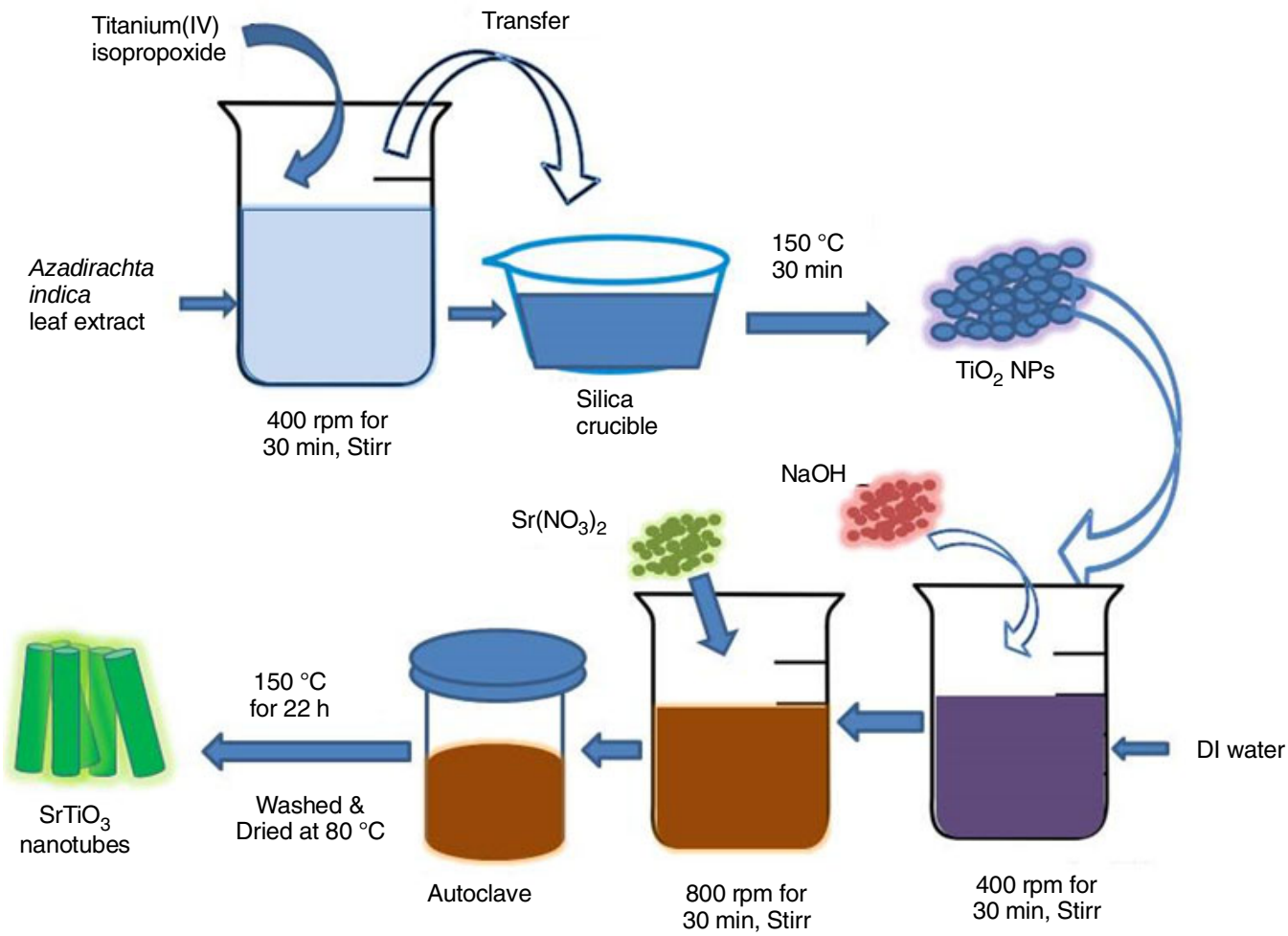

Fig. 1. Synthesis process schematic representation of TiO_2 nanoparticles and $SrTiO_3$ nanotubes

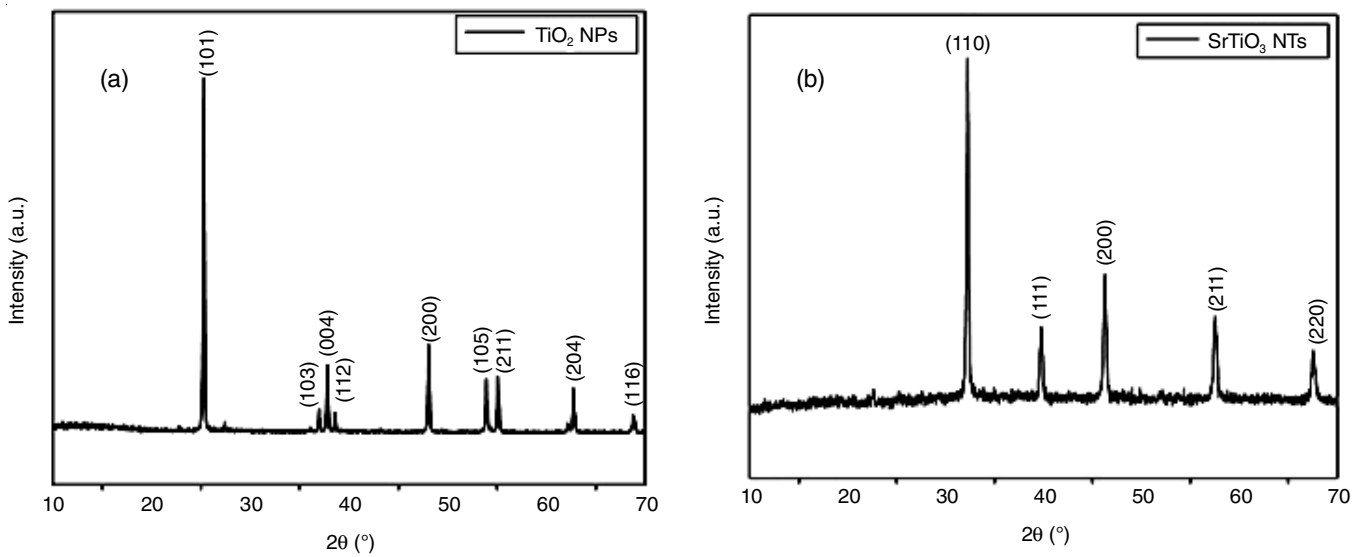

Fig. 2. XRD pattern (a) as-synthesized TiO_2 NPs, (b) as-synthesized $SrTiO_3$ NTs

SEM and EDAX analysis: The as-synthesized TiO_2 nanoparticles were subjected to SEM and EDAX to analyze the elemental composition atomic percentage and size/shape/surface morphology as shown in Fig. 3a-c. SEM micrograph of TiO_2 nanoparticles with different magnifications depicts the dense agglomeration with irregular shape and size (Fig. 3b-c). The EDAX spectrum was the clear evidence of elemental composition of TiO_2 nanoparticles, which not only confirmed the presence of Ti and O elements but also signified the synthesized material purity (Fig. 3a). TiO_2 nanoparticles in SEM micrograph

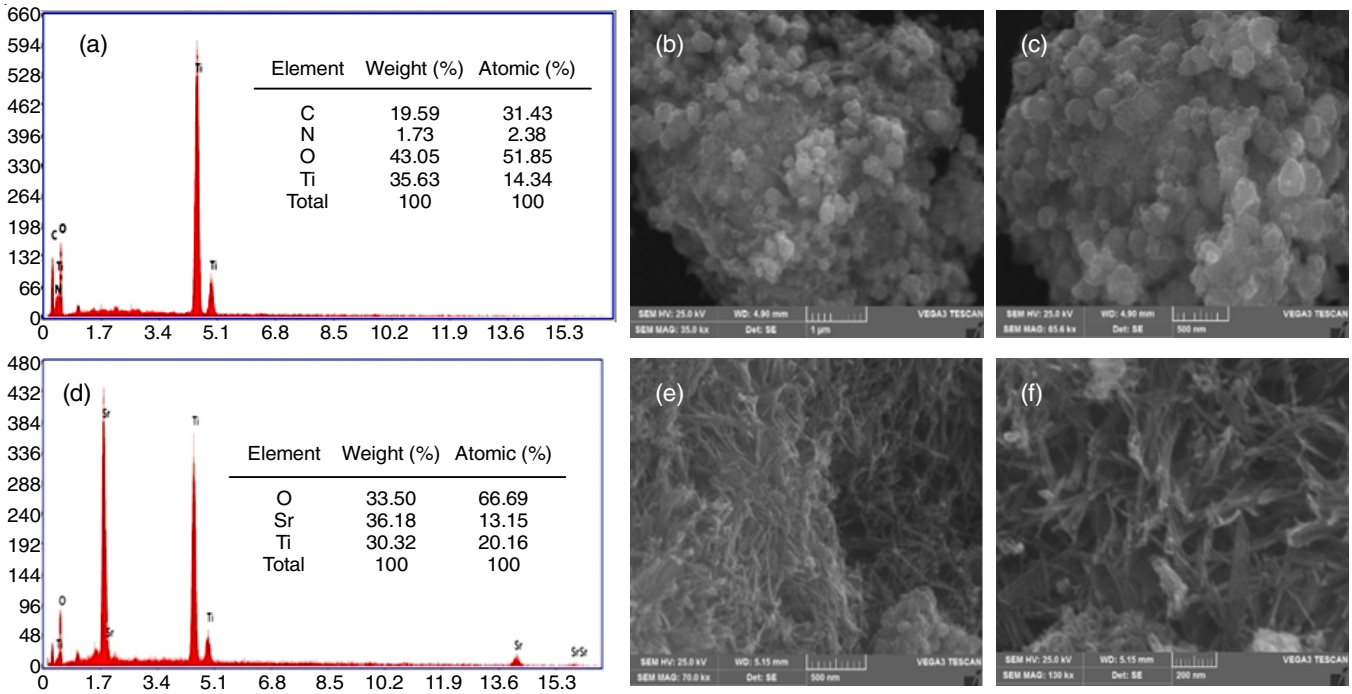

Fig. 3. EDAX-SEM studies of TiO_2 nanoparticles and $SrTiO_3$ nanotubes: EDAX images: (a) as-synthesized TiO_2 nanoparticles, (d) as-synthesized $SrTiO_3$ nanotubes, SEM images: (b) & (c) as-synthesized TiO_2 nanoparticles; (e) & (f) as-synthesized $SrTiO_3$ nanotubes

also divulge about a flat texture and granular microstructure, with the minimum surface roughness comprising spherical particles about 70-80 nm in an average. In similar hydrothermally synthesized $SrTiO_3$ nanotubes were exposed to study of elemental composition atomic percentage and size/shape/surface morphology using EDAX and SEM, respectively (Fig. 3d-f). Mesoporous structures of $SrTiO_3$ nanotubes were clearly seen with no templates or additives. The $SrTiO_3$ nanotubes with continuous mesoporous walls were observed from SEM micrograph and these materials with mesoporous generally possess large surface area with various active sites. The formation of $SrTiO_3$ nanotubes in accordance with SEM micrograph showed clear nanotubes formation with no agglomeration at magnification of 200 and 500 nm scale (Fig. 3b-c). The presence of Sr, Ti and O in the sample and their distribution were revealed by the EDAX spectrum and mapping as can be seen in Fig. 3d. The stoichiometric ratio of Sr:Ti was well coordinated with the as-synthesized, which was revealed by the strong Sr and Ti peaks seen in the inset table (Fig. 3d). The high purity was clearly evidenced with EDAX analysis of as-synthesized $SrTiO_3$ nanotubes as per the stoichiometric ratio confirming the absence of any other impurity peaks. The further confirmation of functional groups of TiO_2 nanoparticles and $SrTiO_3$ nanotubes were studied using FTIR analysis, which interprets the elemental composition.

FTIR studies: The FTIR spectra of as-synthesized TiO_2 nanoparticles were recorded using Perkin Elmer Spectrum 2 from 4000 cm^{-1} to 450 cm^{-1} range (Fig. 4a). The peaks at 732 and 485 cm^{-1} confirmed the bonding for O-Ti-O in anatase morphology [25,26] and the broad peak at 1633 cm^{-1} corresponds to the water and hydroxyl groups absorbed on the surface [26]. The peaks obtained at 3360 cm^{-1} is due to stretching vibration of O-H groups in the prepared samples [27] and the weak absorption bands at 2050 and 1987 cm^{-1} represent the C-H stretching modes. Similarly, Fig. 4b represents the FTIR spectra recorded for as-synthesized $SrTiO_3$ nanotubes. The characteristic frequency for $SrTiO_3$ nanotubes were observed at 3361, 2051, 1986, 1640, 543, 457 cm^{-1}. The peaks around 3361 cm^{-1} are due to the absorption of O-H stretching, while the weak absorption bands at 2051 and 1986 cm^{-1} represent C-H stretching modes. The vibrations peaks at 457 cm^{-1} is attributed to Ti-O bending vibrations and the peaks at 1640 and 543 cm^{-1} correspond to C-H bend [28,29].

UV-visible studies: The as-synthesized TiO_2 nanoparticles and $SrTiO_3$ nanotubes were characterized by UV-visible spectra and from that results found the bandgap (E_g) by plotting the $(\alpha h\nu)^2$ *vs.* photon energy (eV), which were matched the reported values. The UV-visible spectra of TiO_2 nanoparticles, $SrTiO_3$ nanotubes are shown in Fig. 5. Both TiO_2 nanoparticles (E_g = 3.2 eV) and $SrTiO_3$ nanotubes (E_g = 3.25 eV) are large band-gap semiconductors [30], an intense absorption for these samples are observed in UV range (wavelength < 400 nm). Conversely, the spectra of TiO_2 nanoparticles and $SrTiO_3$ nanotubes show a small "absorption tail" (Urbach tail) in the visible range, between 500 and 400 nm, as a result of exponential increase of absorption coefficient in the range of absorption edge [31]. Appearance of the absorption tail makes some disturbances in finding of the optical band-gap (E_g) energy from UV-visible spectrum.

TEM studies: The transmission electron microscopy (TEM) technique revealed the crystallographic structure facts of the materials from the images of phase-contrast. In the present work, ethanol was used as dispersion medium for $SrTiO_3$ nanotubes and was then sonicated. Further a droplet was placed

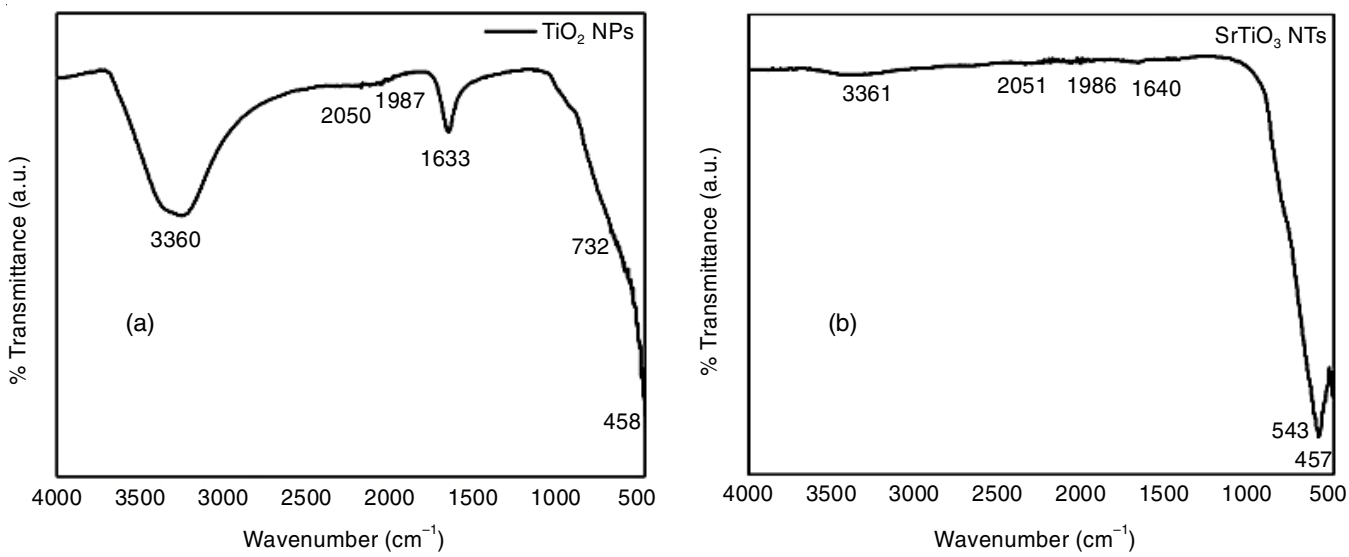

Fig. 4. FTIR profile (a) as-synthesized TiO_2 nanoparticles, (b) as-synthesized $SrTiO_3$ nanotubes

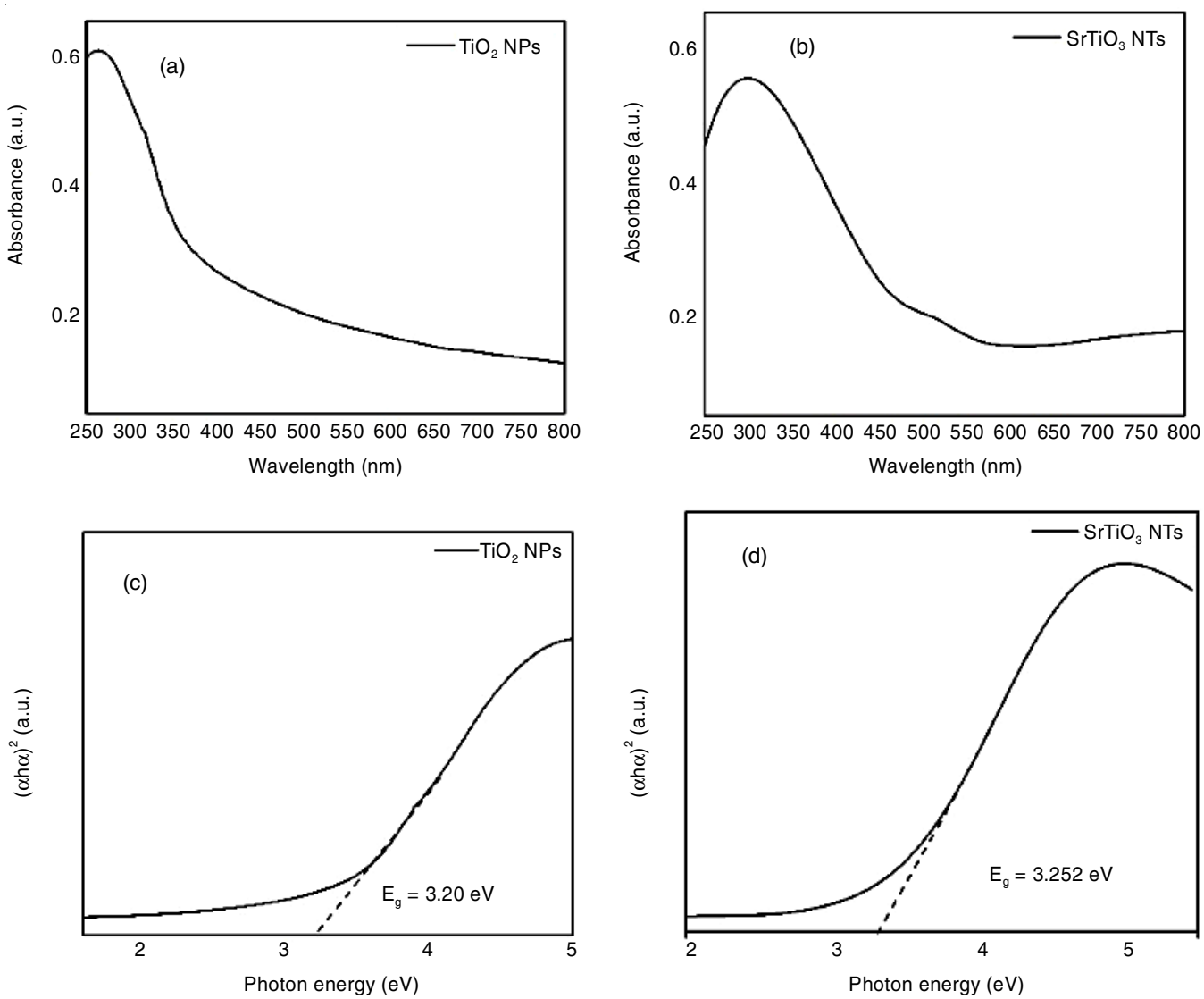

Fig. 5. UV-vis spectra absorbance *vs.* wavelength (nm) of (a) TiO_2 nanoparticles (b) $SrTiO_3$ nanotubes, optical bandgap plot $(\alpha h\nu)^2$ *vs.* photon energy (eV) from UV-vis spectra of (c) TiO_2 nanoparticles (d) $SrTiO_3$ nanotubes

onto carbon-coated copper grid (400 mesh) and dried. The sample was then subjected to TEM and the obtained image from the sample has been shown in Fig. 6a-b. From the TEM image and SAED pattern (Fig. 6c-d), the *d*-spacings of the (110) crystallographic planes of cubic $SrTiO_3$ was well in consistent with the interplanar spacing (~0.27 nm). Similarly, the *d*-spacings of the crystallographic planes (111), (211), (220) and (101) between lattice planes were well matched with obtained XRD pattern as indicated in Fig. 6d. The TEM images of $SrTiO_3$ were clearly evidenced the nanotube formation (~12 nm diameter and ~70 nm length) with number of irregular orientations (Fig. 6b).

Photocatalytic degradation of methylene blue dye: The photocatalytic activity of as-synthesized $SrTiO_3$ nanotubes was investigated for phase decomposition (aqueous) of methylene blue dye in the presence of natural sunlight irradiation and UV irradiation at ambient temperature and the comprehensive study was compared with TiO_2 nanoparticles. The adsorption-desorption equilibrium was attained by monitoring the adsorption of methylene blue in double distilled water using the $SrTiO_3$ catalyst maintaining the dark conditions for 150 min was recorded using UV-visible absorption spectra as shown in Fig. 7f-g for UV light and visible light, respectively. The adsorption of methylene blue showed the enhanced photocatalytic activity which might be due to $SrTiO_3$ nanotubes molecular interaction with methylene blue when exposed to sunlight and UV light. Prior to illumination, 30 mg photocatalyst was added to the methylene blue solution with 30ppm concentration. In a typical experiment, 30 mg of photocatalyst was dispersed in 500 mL of double distilled water to which 30 ppm methylene blue dye was added to form the resultant solution. This resultant mixture was stirred dynamically using magnetic stirrer at 600 rpm for 90 min and the degraded solution were collected at regular interval of time period say 15 min and degradation efficiency (n) was measured using formula:

$$n = \frac{(1-C)}{C_o} \quad (1)$$

where, C_o is the initial concentration before irradiation with light and C is the concentration of dye after irradiation time. The photocatalytic activities of $SrTiO_3$ nanotubes were inspected

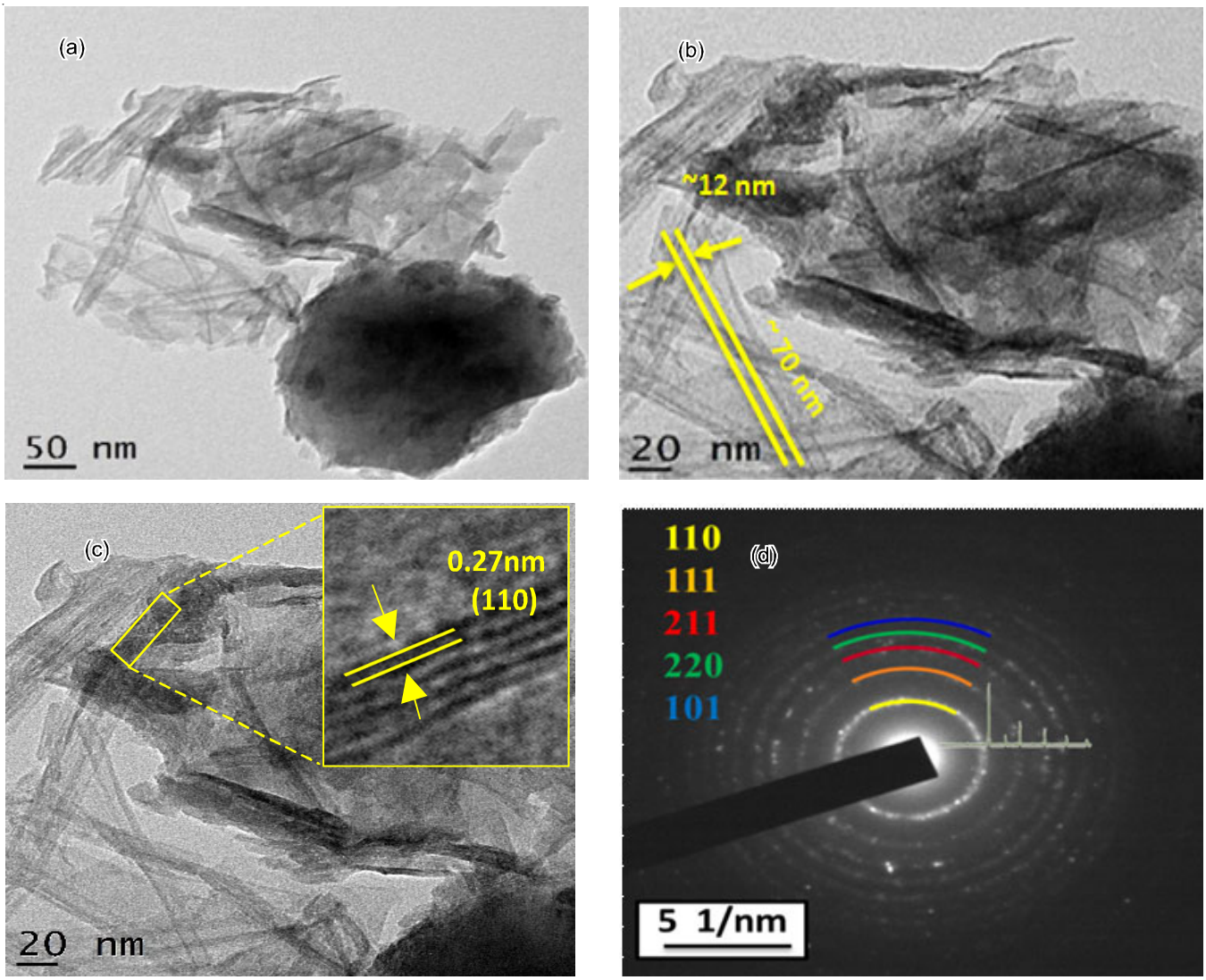

Fig. 6. TEM images (a) as-synthesized $SrTiO_3$ nanotubes at 50 nm magnification, (b) as-synthesized $SrTiO_3$ nanotubes at 20 nm magnification, (c) d-spacing of the (110) crystallographic planes of cubic $SrTiO_3$ nanotubes (d) SAED pattern (scale 5 1/nm)

on the photocatalytic degradation of methylene blue dye under visible light illumination and UV light. The absorption was 0.98 a.u. for every 15 min and was then gradually decreased finally to 0.128 a.u. for 150 min (UV) and the initial absorbance was 0.98 a.u. was reduced to 0.316 a.u. after visible light illumination for 150 min, which was much better photocatalytic activity with respect to time compared to the earlier reported [12]; the absorption rate constant was plotted for the same (Fig. 7c), the absorbance (a.u.) *vs.* wavelength (nm) was plotted (Fig. 7d).

The degradation efficiency 87% of methylene blue was analyzed using UV-visible spectrophotometer and the peaks

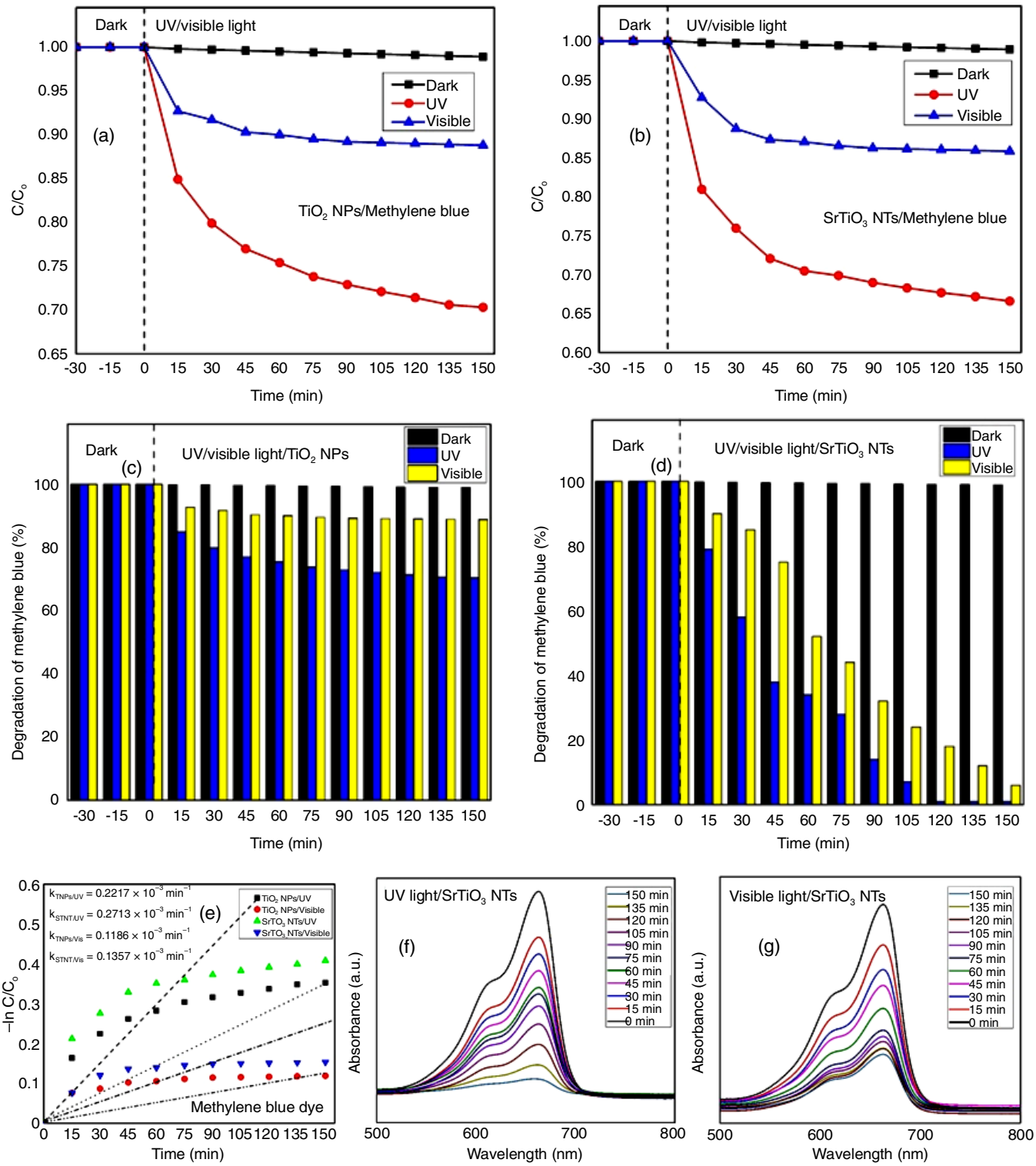

Fig. 7. (a) & (b) Concentration C/C_0 *vs.* irradiation time (min) of TiO_2 nanoparticles & $SrTiO_3$ nanotubes respectively, (b) Percentage degradation *vs.* time (min) of TiO_2 nanoparticles and $SrTiO_3$ nanotubes respectively, (c) absorption rate plot for both, (f) & (g) absorbance (a.u.) *vs.* wavelength (nm) plot ($SrTiO_3$ nanotubes) for UV light and visible light, respectively

observed at 664 nm were assigned as the absorption of π-system [32-40], the concentration versus irradiation time plot for TiO_2 nanoparticles (Fig. 7a) and for $SrTiO_3$ nanotubes (Fig. 7b), percentage degradation *versus* time was plotted for TiO_2 nanoparticles (Fig. 7c) and for $SrTiO_3$ nanotubes (Fig. 7d) and the absorption rate constant for both TiO_2 and $SrTiO_3$ was plotted (Fig. 7e) and absorbance (a.u.) *versus* wavelength (nm) was recorded (Fig. 7f-g) for UV light and visible light, respectively.

Reusability of $SrTiO_3$ nanotubes for methylene blue degradation: The $SrTiO_3$ nanotubes was assessed for its reusability in order to prove the capability as photocatalyst and maintained at more than 80%, which showed its durability (Fig. 8). The $SrTiO_3$ nanotubes was collected after the photocatalytic degradation and sonicated in ultra sonicator for 10 min and washed for 3-4 times with deionized water and with ethyl alcohol, followed by drying in an oven at 80 ºC overnight. Then, catalyst was disbursed to act as photocatalyst for consequent cycles to run in the removal process. The $SrTiO_3$ nanotubes was examined for the catalytic activity was tested under natural sunlight irradiation at ambient temperature. In all the four cycles efficiencies of removal of methylene blue dye was 93.5, 87.2, 83.9 and 80.7%, respectively evidently proved the consistency of $SrTiO_3$ nanotubes for the removal of methylene blue dye.

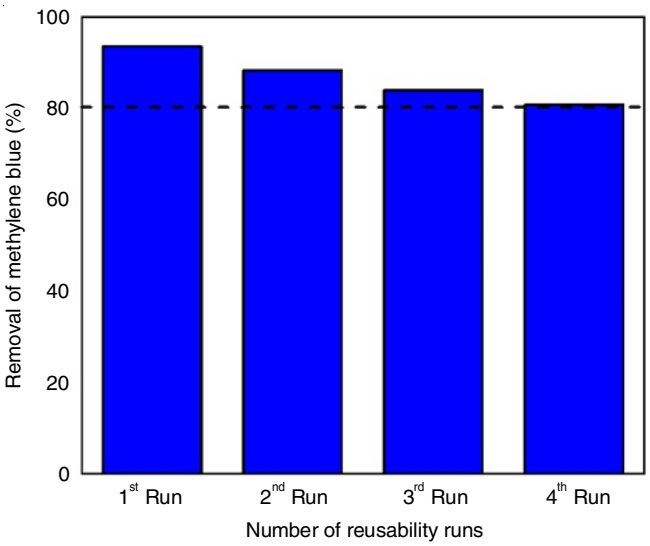

Fig. 8. Reusability tests for $SrTiO_3$ nanotubes the photocatalytic degradation of methylene blue

Conclusion

The green synthesized TiO_2 nanoparticles were successfully employed in synthesis of effective $SrTiO_3$ nanotubes as photocatalyst using hydrothermal method at 150 ºC and its determination of chemical composition, purity, shape, surface morphology were proficiently analyzed using various analytical methods. The as-synthesized $SrTiO_3$ nanotubes (~12 nm diameter) with energy bandgap of 3.25 eV (purest form of semiconductor) were investigated using photocatalytic activity for phase decomposition (aqueous) of methylene blue dye under natural sunlight irradiation at ambient temperature and is compared with TiO_2 nanoparticles for comprehensive analysis. The degradation efficiency of 87% ($SrTiO_3$ nanotubes) was evident from the obtained results of methylene blue dye degradation under UV irradiation and visible light illumination (150 min) showed the better photocatalytic property as compared to the earlier reported literature. Reusability tests clearly evidenced the $SrTiO_3$ nanotubes towards the consistency of photocatalyst with greater durability and the percentage removal of dye was 80.7% even after the run of 4th cycle. The results show the usage of photocatalyst in terms good reusability and effective wastewater treatment proving $SrTiO_3$ nanotubes to be a promising material in the field of catalysis and optics.

ACKNOWLEDGEMENTS

The authors acknowledge Department of Science and Technology-Science and Engineering Research Board, Government of India for the financial support for carryout the experiment (File no. SB/EMEQ-171/2014).

CONFLICT OF INTEREST

The authors declare that there is no conflict of interests regarding the publication of this article.

REFERENCES

1. M. Ye, M. Wang, D. Zheng, N. Zhang, C. Lin and Z. Lin, *Nanoscale*, **6**, 3576 (2014); https://doi.org/10.1039/C3NR05564G
2. D. Wang, J. Ye, T. Kako and T. Kimura, *J. Phys. Chem. B*, **110**, 15824 (2006); https://doi.org/10.1021/jp062487p
3. G. Zhang, G. Liu, L. Wang and J.T.S. Irvine, *Chem. Soc. Rev.*, **45**, 5951 (2016); https://doi.org/10.1039/C5CS00769K
4. Q. Chen, N. De Marco, Y.M. Yang, T.-B. Song, C.-C. Chen, H. Zhao, Z. Hong, H. Zhou and Y. Yang, *Nano Today*, **10**, 355 (2015); https://doi.org/10.1016/j.nantod.2015.04.009
5. M. Moniruddin, B. Ilyassov, X. Zhao, E. Smith, T. Serikov, N. Ibrayev, R. Asmatulu and N. Nuraje, *Mater. Today Energy*, **7**, 246 (2018); https://doi.org/10.1016/j.mtener.2017.10.005
6. M. Petrovic, V. Chellappan and S. Ramakrishna, *Sol. Energy*, **122**, 678 (2015); https://doi.org/10.1016/j.solener.2015.09.041
7. K. Mahmood, S. Sarwar and M.T. Mehran, *RSC Adv.*, **7**, 17044 (2017); https://doi.org/10.1039/C7RA00002B
8. H. Shen, Y. Lu, Y. Wang, Z. Pan, G. Cao, X. Yan and G. Fang, *J. Adv. Ceramics*, **5**, 298 (2016); https://doi.org/10.1007/s40145-016-0203-3
9. W. Zhao, J. Zhang, J. Pan, J. Qiu, J. Niu and C. Li, *Nanoscale Res. Lett.*, **12**, 371 (2017); https://doi.org/10.1186/s11671-017-2130-9
10. T. Klaytae, P. Panthong and S. Thountom, *Ceram. Int.*, **39**, S405 (2013); https://doi.org/10.1016/j.ceramint.2012.10.103
11. W. Rheinheimer and M.J. Hoffmann, *J. Mater. Sci.*, **51**, 1756 (2016); https://doi.org/10.1007/s10853-015-9535-6
12. D. Hou, X. Hu, W. Ho, P. Hu and Y. Huang, *J. Mater. Chem. A Mater. Energy Sustain.*, **3**, 3935 (2015); https://doi.org/10.1039/C4TA05485G
13. A. Fujishima and K. Honda, *Nature*, **238**, 37 (1972); https://doi.org/10.1038/238037a0
14. M.S. Wrighton, A.B. Ellis, P.T. Wolczanski, D.L. Morse, H.B. Abrahamson and D.S. Ginley, *J. Am. Chem. Soc.*, **98**, 2774 (1976); https://doi.org/10.1021/ja00426a017
15. G. Canu and V. Buscaglia, *CrystEngComm*, **19**, 3867 (2017); https://doi.org/10.1039/C7CE00834A

16. L. Chen, S. Zhang, L. Wang, D. Xue and S. Yin, *J. Cryst. Growth*, **311**, 746 (2009); https://doi.org/10.1016/j.jcrysgro.2008.09.185
17. S. Shoji, G. Yin, M. Nishikawa, D. Atarashi, E. Sakai and M. Miyauchi, *Chem. Phys. Lett.*, **658**, 309 (2016); https://doi.org/10.1016/j.cplett.2016.06.062
18. K. Domen, A. Kudo, T. Onishi, N. Kosugi and H. Kuroda, *J. Phys. Chem.*, **90**, 292 (1986); https://doi.org/10.1021/j100274a018
19. S. Burnside, J.E. Moser, K. Brooks, M. Gratzel and D. Cahen, *J. Phys. Chem. B*, **103**, 9328 (1999); https://doi.org/10.1021/jp9913867
20. J.H. Pan, C. Shen, I. Ivanova, N. Zhou, X. Wang, W.C. Tan, Q.-H. Xu, D.W. Bahnemann and Q. Wang, *ACS Appl. Mater. Interfaces*, **7**, 14859 (2015); https://doi.org/10.1021/acsami.5b03396
21. S.T. Huang, W.W. Lee, J.L. Chang, W.S. Huang, S.Y. Chou and C.C. Chen, *J. Taiwan Inst. Chem. Eng.*, **45**, 1927 (2014); https://doi.org/10.1016/j.jtice.2014.02.003
22. D. Chen, X. Jiao and M. Zhang, *J. Eur. Ceram. Soc.*, **20**, 1261 (2000); https://doi.org/10.1016/S0955-2219(00)00003-0
23. C.E. Ekuma, M. Jarrell, J. Moreno and D. Bagayoko, *AIP Adv.*, **2**, 012189 (2012); https://doi.org/10.1063/1.3700433
24. E.C. Su, B.S. Huang and M.Y. Wey, *Sol. Energy*, **134**, 52 (2016); https://doi.org/10.1016/j.solener.2016.04.007
25. G. Soler-Illia, A. Louis and C. Sanchez, *Chem. Mater.*, **14**, 750 (2002); https://doi.org/10.1021/cm011217a
26. J.C. Yu, L.Z. Zhang, Z. Zheng and J.C. Zhao, *Chem. Mater.*, **15**, 2280 (2003); https://doi.org/10.1021/cm0340781
27. W.R. Kunusa, R. Abdullah, K. Bilondatu and W.Z. Tulie, *J. Phys. Conf. Ser.*, **1422**, 012040 (2020); https://doi.org/10.1088/1742-6596/1422/1/012040
28. T. Sakthivel and K. Jagannathan, *Mechan. Mater. Sci. Eng. J.*, **9(1)** (2017); https://doi.org/10.2412/mmse.80.76.610
29. H. Turasan and J.L. Kokini, *Biomacromolecules*, **18**, 331 (2017); https://doi.org/10.1021/acs.biomac.6b01455
30. Y. Du, M.S. Zhang, J. Wu, L. Kang, S. Yang, P. Wu and Z. Yin, *Appl. Phys. Mater. Sci.*, **76**, 1105 (2003); https://doi.org/10.1007/s00339-002-1998-z
31. F. Urbach, *Phys. Rev.*, **92**, 1324 (1953); https://doi.org/10.1103/PhysRev.92.1324
32. G. Liu, T. Wu, J. Zhao, H. Hidaka and N. Serpone, *Environ. Sci. Technol.*, **33**, 2081 (1999); https://doi.org/10.1021/es9807643
33. C. Ramli, P. Ismail and A. Rahmat, *Scient. World J.*, **2014**, 964731 (2014); https://doi.org/10.1155/2014/964731
34. A. Shi, H. Li, S. Yin, B. Liu, J. Zhang and Y. Wang, *Appl. Catal. B*, **218**, 137 (2017); https://doi.org/10.1016/j.apcatb.2017.06.017
35. T. Xian, H. Yang, L. Di, J. Ma, H. Zhang and J. Dai, *Nanoscale Res. Lett.*, **9**, 327 (2014); https://doi.org/10.1186/1556-276X-9-327
36. B. Ganapuram, M. Alle, R. Dadigala, A. Dasari, V. Maragoni and V. Guttena, *Int. Nano Lett.*, **5**, 215 (2015); https://doi.org/10.1007/s40089-015-0158-3
37. D. Ayodhya, M. Venkatesham, A. Santoshi kumari, G.B. Reddy, D. Ramakrishna and G. Veerabhadram, *J. Exp. Nanosci.*, **11**, 418 (2016); https://doi.org/10.1080/17458080.2015.1070312
38. J. Fan, Z. Zhao, W. Liu, Y. Xue and S. Yin, *J. Colloid Interface Sci.*, **470**, 229 (2016); https://doi.org/10.1016/j.jcis.2016.02.045
39. N.K. Veldurthi, S. Palla, R. Velchuri, P. Guduru and V. Muga, *Mater. Express*, **5**, 445 (2015); https://doi.org/10.1166/mex.2015.1255
40. P. Wongkalasin, S. Chavadej and T. Sreethawong, *Colloids Surf. A Physicochem. Eng. Asp.*, **384**, 519 (2011); https://doi.org/10.1016/j.colsurfa.2011.05.022